Binding Energies and ^{19}F Nuclear Magnetic Deshielding in Paramagnetic Halogen-Bonded Complexes of TEMPO with Haloperfluorocarbons

Carlo Cavallotti,* Pierangelo Metrangolo,* Franck Meyer, Francesco Recupero, and Giuseppe Resnati*

Dipartimento di Chimica, Materiali ed Ingegneria Chimica "G. Natta", Politecnico di Milano, Via Mancinelli 7−20131 Milano, Italy

Received: April 28, 2008; Revised Manuscript Received: July 08, 2008

^{19}F NMR measurements and theoretical calculations were performed to study paramagnetic complexes of iodoperfluorocarbons with stable nitroxide radicals. Contrary to what is usually measured for diamagnetic halogen-bonded complexes involving iodoperfluorocarbons, it was found that the formation of complexes with the 2,2,6,6-tetramethyl(piperidin-1-yloxyl) (TEMPO) radical determines downfield shifts in the ^{19}F NMR spectra. The experimental finding was confirmed by calculating nuclear shielding using density functional theory and correcting the isotropic diamagnetic ^{19}F chemical shift with contact interactions evaluated from the hyperfine coupling tensor. The computational analysis of the interaction between CF_3I and TEMPO, by using DFT and MP2 theories, showed that the occurrence of the halogen bond between the interacting partners is associated with a significant charge transfer to CF_3I and that the measured downfield shift is due to the occurring spin transfer.

1. Introduction

Halogen atoms are typically located at the periphery of organic molecules and are thus ideally positioned to be involved in intermolecular interactions. Theoretical studies predict, and experimental results confirm, that halogen atoms give rise to a wide diversity of interactions, which may differ from each other from the physical and chemical properties point of view. For instance, as far as the polar character is concerned, halogen atoms show an amphoteric character and function as the electron donor sites (Lewis bases) when interacting in a direction perpendicular to the axis of the covalent bond they are involved in[1,2] and as the electron acceptor sites (Lewis acids) when interacting on the extension of the axis of that covalent bond.[3−7] This latter type of interaction is named halogen bonding (XB) (by analogy to hydrogen bonding with which it shares numerous properties) and has recently attracted increasing interest as a reliable and powerful tool to design and control intermolecular recognition phenomena.[8−12]

Halocarbons have been effectively used to form halogen-bonded adducts in the solid, liquid, and gas phases and the more electron-poor the halogen atom is, the more pronounced its tendency to interact with electron donor partners. Thanks to the electron-withdrawing ability of fluorine atoms, iodoperfluorocarbons (PFCs), and to a lesser extent bromo-PFCs, give rise to particularly strong halogen bonds when interacting with a large variety of lone pair possessing atoms, either neutral or anionic (e.g., amine, imine, and pyridine nitrogens, ether, carbonyl, sulfinyl, and phosphonyl oxygens, as well as halide, cyanide, and thiocyanate anions).[8−11]

^{19}F NMR is an extremely useful tool to investigate intermolecular recognition processes involving fluorine-substituted modules, thanks to its large chemical shift range and its high intrinsic sensitivity (85% of ^{1}H). We have already showed that XB causes large changes in the ^{19}F NMR chemical shifts of halo-PFCs and that this phenomenon may provide thermodynamic data accompanying complex formation. As XB is weaker than covalent bonds, it is reasonable to discuss ^{19}F NMR spectra of the obtained adducts in terms of modified signals of starting perfluorinated components. The basic character of different electron-donating moieties toward halogen electron acceptors in bromo- and iodoperfluoroalkanes (PFAs) can be qualitatively anticipated from the extent of the shift induced on the $-CF_2X$ signals. In particular, in iodo-, bromo-, and chloro-PFAs the signal of the fluorine atom(s) geminal to the iodine, bromine, and chlorine invariably shows a high-field shift on XB formation, and chemical shifts changes as large as 10−20 ppm are observed with the strongest electron donors. In haloperfluoroarenes the fluorine atoms ortho to the heavy halogen atom also show a high-field shift on XB formation, but the effect is less remarkable. This is also the case for fluorine atoms vicinal, rather than geminal, to the halogen atom in halo-PFAs, the upfield shift clearly decreasing on increasing the distance between the probed fluorine and the halogen-bonded site.[13,14]

Nitroxide free radicals are extensively used for developing molecular magnetic materials, and some papers describe how their oxygen atoms function as XB acceptor site (electron donors).[15−17] Unequivocal structural proofs of this ability have been obtained from X-ray analysis,[18−20] and either ferromagnetic or antiferromagnetic properties have been observed.[21−23] We have already reported how a redistribution of spin density occurs when nitroxide free radicals are involved in XB formation.[24] In this paper we describe how unique changes of ^{19}F NMR spectra of the halo-PFCs result when such a spin density transfer occurs upon XB formation with nitroxide free radicals. In sharp contrast with the upfield shifts typically observed for nonradical electron donors, 2,2,6,6-tetramethyl(piperidin-1-yloxyl) radical (TEMPO) induces a much larger downfield shift of the signal of the fluorine atoms geminal to the iodine and bromine of halogen-bonded iodo- and bromo-PFAs. The key relevance of XB to the observed changes in ^{19}F NMR spectra of the halo-

* Corresponding authors. E-mail: carlo.cavallotti@polimi.it (C.C.); pierangelo.metrangolo@polimi.it (P.M.); giuseppe.resnati@polimi.it (G.R.). Phone: +39 02 2399 3176. Fax: +39 02 2399 3180.

10.1021/jp803685r CCC: $40.75
Published on Web 09/17/2008

SCHEME 1: Formation of the PMPIP−Halo-PFC Complex

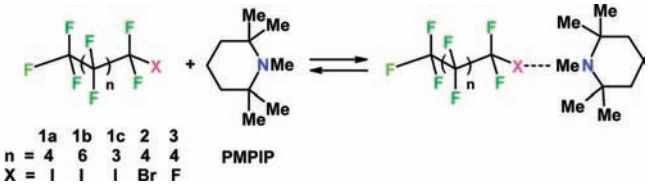

SCHEME 2: Formation of the TEMPO−Halo-PFC Complex

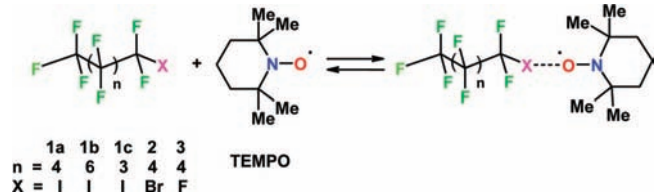

PFCs is unequivocally proven by the decrease of the changes observed with increasing distance from the halogen atom involved in XB in long-chain halo-PFAs. As a result of the transfer of some of the unpaired spin density from the nitroxidic moiety through the halogen atom, a strong and specific paramagnetic shift is observed on the signals of the fluorine atoms geminal to the iodine and bromine of halogen-bonded iodo- and bromo-PFAs. This strong and specific paramagnetic shift can be clearly distinguished from the not specific one observed on the signals of the fluorine atoms far from the halogen-bonded site, and, in general, in the ^{19}F NMR spectra of nonfunctionalized PFCs.

The general features of XB can now be predicted with reasonable accuracy through computational studies, but it is still challenging to develop models accurate enough to predict spectroscopic effects. This is particularly true with iodine derivatives where high-quality basis sets are not readily available and are computationally expensive. Here we report also a theoretical analysis of the origin of the strong and specific paramagnetic effect observed upon interaction of TEMPO with iodo-PFCs.

2. Results and Discussion

2.1. ^{19}F NMR. Typically, the ^{19}F NMR spectra of halo-PFCs in the presence of trace amounts of electron-donating compounds cannot be distinguished from those of the pure halo-PFCs. On the other hand, by increasing the concentration of the donor species, progressively larger shifts of the ^{19}F signals are observed, which, on dilution, return to the initial chemical shifts, and no signal splitting or broadening has ever been observed. These findings are consistent with a donor−acceptor association equilibrium, which is rapid at room temperature on the NMR time scale (Scheme 1). In order to shift this equilibrium toward the complexation of the electron acceptor, and to maximize the chemical shift effects, in the experiments described in this article the electron donor/acceptor ratio was varied in the range of 1:1, 3:1, 6:1, 9:1, and 12:1.

The ^{19}F NMR spectra of 1-iodo-, 1-bromo-, and of perfluorohexane, (**1a**), (**2**), and (**3**), respectively, have been recorded in the presence of 1,2,2,6,6-pentamethylpiperidine (PMPIP), as prototype neutral and diamagnetic electron donor molecule. The chemical shift differences of the $-CF_2-$ group signals between the values observed in a noncoordinating solvent ($CDCl_3$) and those recorded in $CDCl_3$ solutions containing the electron donor module ($\Delta\delta_{\text{used electron donor}} = \delta_{CDCl_3} - \delta_{\text{used electron donor}}$) are reported in Table 1. Clearly, the XB between the electron deficient iodine or bromine atoms of the halo-PFCs and the N atom of PMPIP strongly influences the signals of the $-CF_2-X$ groups and gives rise to detectable upfield shifts of the ^{19}F NMR resonances. A $\Delta\delta$ value of 0.41 ppm (run 5) was measured in the case of the iodide **1a**, when the ratio PMPIP/**1a** was 12:1.

Quantum chemical calculations, as well as experimental data in the solid, solution, and gas phases, show that the halogen-bonding energy decreases moving from iodine to bromine to chlorine following the order of the halogen atom polarizability and consistent with a key role of halogen polarization (and/or charge-transfer energies) in the interaction.[7] This trend is confirmed also by the values measured for the interaction between PMPIP and perfluorohexyl bromide **2**, which are reported in Table 1. In fact, the $\Delta\delta_{-CF2Br}$ values measured for perfluorohexyl bromide in the presence of increasing amounts of PMPIP were invariably smaller than the ones measured for its iodo analogue. The maximum $\Delta\delta$ value measured was of 0.06 ppm (run 5) in the case of a PMPIP/**2** ratio of 12:1. This value is only a little higher than the $\Delta\delta$ values observed for the other $-CF_2-$ and $-CF_3$ groups in the perfluoroalkyl chain.

The observed chemical shift changes were mainly caused by the formation of halogen bonding. Indeed, shifts of the signals of the $-CF_2-$ group geminal to the iodine and bromine atoms are invariably larger than the shifts of the other $-CF_2-$ groups, these shifts decreasing with increasing distance from the electron acceptor iodine and bromine atoms. The minor role played by "generic" solvent effects (nonspecific solute−solvent interactions) in inducing the observed $\Delta\delta_{-CF2-}$ values is further confirmed by the resulting $\Delta\delta_{-CF2-}$ values measured for perfluorohexane (**3**) in the same conditions and listed in Table 1.

In the absence of the iodine or bromine atoms specifically involved in the intermolecular interaction, randomly distributed minor upfield, or downfield shifts in some cases, occur, and they are comparable with those observed for the internal difluoromethylene groups in the iodo- and bromo derivatives **1a** and **2**. These "generic" contributions are at least 1 order of magnitude smaller than the $\Delta\delta_{-CF2X}$ value in **1a**. The observed

TABLE 1: Chemical Shift Differences ($\Delta\delta$,ppm) of 1-Iodoperfluorohexane (1a, X = I), 1-Bromoperfluorohexane (2, X = Br), and Perfluorohexane (3, X = F) in $CDCl_3$ on Increasing the Amount of Electron Donor (PMPIP)[a]

		$\Delta\delta_{XCF2CF2CF2-}$			$\Delta\delta_{XCF2CF2CF2-}$			$\Delta\delta_{XCF2CF2CF2-}$			$\Delta\delta_{CF3CF2CF2-}$		
run	solvent	**1a**	**2**	**3**	**1a**	**2**	**3**	**1a**	**2**	**3**	**1a**	**2**	**3**
1	PMPIP: 1 equiv	+0.0580	+0.0062	+0.0040	+0.0100	+0.0034	+0.0090	+0.0019	+0.0059	+0.0030	+0.063	+0.0056	+0.0040
2	PMPIP: 3 equiv	+0.1205	+0.0153	+0.0170	+0.0219	+0.0098	+0.0190	+0.011	+0.0121	+0.0160	+0.0159	+0.0122	+0.0170
3	PMPIP: 6 equiv	+0.2162	+0.029	+0.0260	+0.0406	+0.0219	+0.0290	+0.0242	+0.0224	+0.0260	+0.0314	+0.0250	+0.0260
4	PMPIP: 9 equiv	+0.3161	+0.0451	+0.0390	+0.0605	+0.0326	+0.0390	+0.0391	+0.0325	+0.0380	+0.048	+0.0383	+0.0390
5	PMPIP: 12 equiv	+0.4130	+0.0615	+0.0490	+0.0796	+0.0453	+0.0510	+0.0533	+0.0445	+0.0510	+0.0641	+0.0516	+0.0490

[a] $\Delta\delta_{\text{used electron donor}} = \delta_{CDCl_3} - \delta_{\text{used electron donor}}$.

TABLE 2: Chemical Shift Differences ($\Delta\delta$, ppm) of 1-Iodoperfluorohexane (1a, X = I), 1-Bromoperfluorohexane (2, X = Br), and Perfluorohexane (3, X = F) in $CDCl_3$ on Increasing the Amount of Electron Donor (TEMPO)[a]

		$\Delta\delta_{XCF_2CF_2CF_2-}$			$\Delta\delta_{XCF_2CF_2CF_2-}$			$\Delta\delta_{XCF_2CF_2CF_2-}$			$\Delta\delta_{CF_3CF_2CF_2-}$		
run	solvent	**1a**	**2**	**3**	**1a**	**2**	**3**	**1a**	**2**	**3**	**1a**	**2**	**3**
1	TEMPO: 1 equiv	−0.52	−0.34	−0.25	−0.29	−0.29	−0.22	−0.27	−0.28	−0.24	−0.30	−0.32	−0.25
2	TEMPO: 3 equiv	−1.72	−1.03	−0.84	−0.92	−0.88	−0.73	−0.86	−0.84	−0.79	−0.96	−0.96	−0.84
3	TEMPO: 6 equiv	−3.50	−2.05	−1.75	−1.87	−1.75	−1.52	−1.7	−1.67	−1.64	−1.94	−1.90	−1.75
4	TEMPO: 9 equiv	−5.36	−3.07	−2.69	−2.86	−2.62	−2.34	−2.68	−2.50	−2.51	−2.98	−2.85	−2.69
5	TEMPO: 12 equiv	−7.22	−4.15	−3.70	−3.86	−3.54	−3.23	−3.61	−3.38	−3.46	−4.03	−3.85	−3.70

[a] $\Delta\delta_{\text{used electron donor}} = \delta_{CDCl_3} - \delta_{\text{used electron donor}}$.

TABLE 3: Chemical Shift Differences ($\Delta\delta$, ppm) of 1-Iodoperfluorooctane (1b, X = I) and 1-Iodoperfluoropropane (1c, X = I) in $CDCl_3$ on Increasing the Amount of Electron Donor (TEMPO)[a]

		$\Delta\delta_{XCF_2CF_2-}$		$\Delta\delta_{XCF_2CF_2-}$		$\Delta\delta_{CF_3CF_2-}$	
run	solvent	**1b**	**1c**	**1b**	**1c**	**1b**	**1c**
1	TEMPO: 1 equiv	−0.54	−0.50	−0.30	−0.30	−0.31	−0.32
2	TEMPO: 3 equiv	−1.62	−1.65	−0.87	−0.95	−0.91	−1.01
3	TEMPO: 6 equiv	−3.27	−3.36	−1.75	−1.93	−1.83	−2.03
4	TEMPO: 9 equiv	−5.00	−5.12	−2.68	−2.93	−2.79	−3.09
5	TEMPO: 12 equiv	−6.64	−6.77	−3.56	−3.87	−3.72	−4.08

[a] $\Delta\delta_{\text{used electron donor}} = \delta_{CDCl_3} - \delta_{\text{used electron donor}}$.

shifts in the ^{19}F NMR spectra of **3** can be ascribed to an isotropic solvation that can be firmly distinguished from the strong, directional, and specific interaction involving the electron donor and acceptor sites in XB.

The utility of a nitroxide radical as a paramagnetic shift reagent in proton NMR spectroscopy is well-known, in particular for structural elucidation around the proton donor group and the mode of hydrogen bonding.[25,26] TEMPO is a convenient reagent for inducing large paramagnetic shifts because of its stability, inertness, and relatively high solubility in many organic solvents.[27,28] For this reason we decided to study via ^{19}F NMR the interaction of TEMPO with halo-PFAs **1a**, **2**, and **3** (Scheme 2).

Interestingly, the addition of increasing amounts of TEMPO to a $CDCl_3$ solution of the perfluorohexyl iodide **1a** greatly influences the signal of the $-CF_2-I$ group and gives rise to a substantial downfield shift of the ^{19}F NMR resonance, much larger than the shift observed with PMPIP, which was, moreover, toward higher fields. A maximum $\Delta\delta$ value of −7.22 ppm (run 5) was measured in the case of a TEMPO/**1a** ratio of 12:1 (Table 2). Also the resonances associated with the other $-CF_2-$ and $-CF_3$ groups are strongly influenced by the presence of TEMPO in solution. Downfield shifts spanning the range of −3.56 to −4.03 ppm were measured for the remaining perfluoroalkyl chain, with the last value belonging to the trifluoromethyl terminal group, which showed the higher $\Delta\delta$ value alongside the $-CF_2-I$ signal. Also in the case of the internal fluorine resonances the shifts increased with the concentration of TEMPO in solution likewise to what was observed for the $-CF_2-I$ signal.

Also in the case of TEMPO, the $\Delta\delta_{-CF_2Br}$ values measured for perfluorohexyl bromide **2** were invariably smaller than the ones reported for its iodo analogue **1a**. The maximum $\Delta\delta$ value measured was of −4.15 ppm (run 5) in the case of the TEMPO/**2** ratio of 12:1. This value is very close to the $\Delta\delta$ values observed for the other $-CF_2-$ and $-CF_3$ groups in the perfluoroalkyl chain, which showed values in the range of −3.36 to −3.85, with the second highest value belonging again to the trifluoromethyl terminal group.

The $\Delta\delta$ values of perfluorohexane **3** are also reported in Table 2 in order to further confirm the relevance of the XB to the observed chemical shift changes. Interestingly, $\Delta\delta$ values between −3.23 and −3.70 ppm were measured, with the latter value belonging to the terminal $-CF_3$ group. These findings are the proofs of a generic solute−solvent interaction between the perfluoroalkane **3** and TEMPO, which induces a strong paramagnetic effect of the ^{19}F NMR resonances of **3**. By comparison of this nonspecific paramagnetic shift with the shifts induced on the $-CF_2-X$ groups in **1a** and **2**, we can thus conclude that XB is very effective in increasing the TEMPO induced paramagnetic shift through a strong and specific interaction. The observed effects can be attributed to the transfer of some of the unpaired spin density from the nitroxidic moiety to the perfluorinated chain through the heavy halogen atom, as will be shown in the theoretical section of this paper. This transfer is more effective in the case of iodine as it gives rise to a XB stronger than the one given by the bromine atom.

SCHEME 3: Resonant Forms of the TEMPO Radical

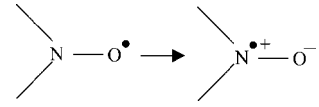

The generality of the concept of using ^{19}F NMR paramagnetic probes to detect the occurrence of attractive noncovalent interactions involving halogen atoms as electrophilic species is demonstrated by the $\Delta\delta$ values listed in Table 3. Also 1-iodoperfluorooctane **1b** and 1-iodoperfluoropropane **1c** upon interaction with TEMPO in $CDCl_3$ solutions show downfield shifts that are very similar in values and trends with the ones observed for **1a** in the same experimental setup. This confirms that we are observing a general effect of the presence of paramagnetic species in solutions of halo-PFCs and that this is a simple, effective, and sensitive tool to detect the formation of halogen-bonded adducts and to establish qualitatively the strength of the interaction. To the best of our knowledge, this is the first report on the use of stable free radicals as ^{19}F NMR spin probes for studying intermolecular interactions involving halo-PFCs.

2.2. DFT and ab Initio Calculations. The origin of the strong and specific paramagnetic effect observed upon interac-

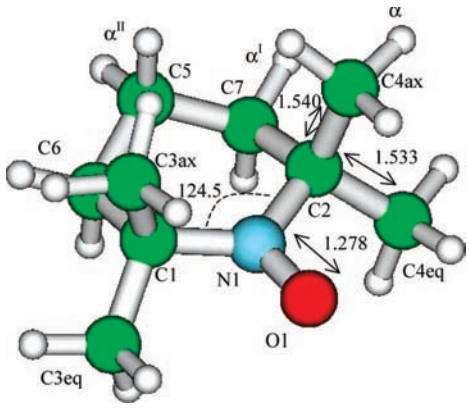

Figure 1. TEMPO structure with labeling of key atoms fully optimized at the B3LYP/aug-cc-pVTZ level. Distances are reported in angstroms and angles in degrees.

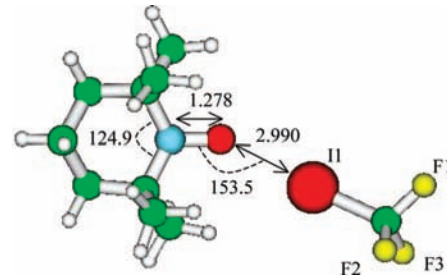

Figure 2. Minimum energy structure of TEMPO in the complex with ICF_3 with labeling of key atoms fully optimized at the aug-cc-pVTZ level. Distances are reported in angstroms and angles in degrees.

tion of TEMPO with halo-PFCs was investigated by means of DFT calculations.

The structure of the considered paramagnetic molecule, TEMPO, is sketched in Figure 1 together with the labeling of nuclei. The minimal energy structure was optimized in vacuum in the *C*1 symmetry group at the unrestricted B3LYP level using two basis sets: the Dunning−Huzinaga double-ζ basis set with added diffuse functions[29] and the aug-cc-pVTZ basis set.[30] A population analysis on the structure determined at the B3LYP/aug-cc-pVTZ level using Mulliken spin densities shows that the unpaired electron is shared between the N1 and the O1 atoms, which have net spin densities of 0.486 and 0.525, respectively. Atomic charges on N1 and O1, determined with a natural population analysis (NPA),[31] are 0.001 and −0.434, respectively. This is usually interpreted describing the electronic structure of TEMPO in terms of two resonant forms, as sketched in Scheme 3.

The C5N structure of the TEMPO ring is similar to the chair conformation of cyclohexane and is characterized by two pairs of axial and equatorial H and CH_3 groups, with distinguishable ^{13}C and undistinguishable ^{1}H chemical shifts.

The effect on ^{19}F NMR chemical shifts when TEMPO is added to a solution containing iodo-PFCs was investigated through DFT and ab initio calculations performed for TEMPO in complex with ICF_3. The structure of the complex was fully optimized at the B3LYP level using two basis sets: the Stuttgart−Dresden effective core potential basis set for iodine and the Dunning−Huzinaga double-ζ basis set for the other atoms (SDD)[29,32] and the Martin/Sundermann SDB-aug-cc-pVTZ basis set with relativistic ECP for iodine[33] and aug-cc-pVTZ for other atoms.[30] The stability of the optimized structures was confirmed by frequency calculations performed at the B3LYP/SDD level. The computed minimum energy structure of the complex TEMPO·ICF_3 is sketched in Figure 2.

The TEMPO·ICF_3 complex structure is characterized by an N1−O1···I1 angle of about 153° and a N−O···I distance of 2.990 Å. This structure is similar to the one determined by Boubekeur et al.,[19] who cocrystallized the 4-amino-2,2,6,6,-tetramethyl(piperidin-1-yloxyl) radical (ATEMPO) with 1,4-diiodo-tetrafluorobenzene (TFDIB). The single-crystal X-ray N−O···I distance is, in fact, 2.827 Å, with a N−O···I angle of 145.0°. This geometrical arrangement was a clear indication of the direct participation of the oxygen lone pairs in the intermolecular bond. Interestingly, differently from what found by Valerio et al.[35] for the ICF_3···NH_3 complex and by Romaniello and Lelj[36] for the CF_3I···$X(CH_3)_n$ (X = N, P, S) adducts, upon binding the I−C distance decreases slightly by 0.005 Å, whereas C−F distances increase by 0.006 Å.

Successively, binding energies, orbital populations, and charge transfers of TEMPO to ICF_3 were calculated by using DFT and MP2 theories and different basis sets. The aim was both to determine the accuracy of the calculations and to investigate the nature of the XB between halo-PFCs and the paramagnetic molecule TEMPO. The results are summarized in Table 4.

The basis sets superposition error (BSSE) is not reported for DFT calculations, for which it was possible to reach the basis set limit by systematically increasing its size. In fact, though the BSSE correction calculated at the B3LYP/SDD level is 1.9 kcal/mol, it drops to 0.1 kcal/mol at the B3LYP/aug-cc-pVTZ level. BSSE corrections for MP2 calculations, evaluated accounting for fragment relaxation,[37,38] are significant for double-ζ basis sets and, as expected, decrease for the aug-cc-pVTZ basis set. All simulations were performed using the G03 computational suite.[39]

Binding energies determined at the unrestricted B3LYP level are sensitive to the size of the basis set. In particular, they decrease from the 7.3 kcal/mol calculated at the B3LYP/SDD level to the 3.2 kcal/mol determined with the largest basis set, on the same geometry. The spin contamination is 0.7543 and 0.7547 at the B3LYP level with the SDD and aug-cc-pVTZ basis sets, respectively. As this is near the value expected for a doublet, we considered the spin contamination error negligible. On the other hand, the binding energies determined using the unrestricted UMP2 theory were significantly different from those calculated at the B3LYP level. In particular, DFT and UMP2 energies calculated with the largest basis set differed by 4 kcal/mol. Since the experimental binding enthalpy measured for the *n*-$C_8F_{17}I$···TEMPO complex is 7 ± 0.4 kcal/mol,[24] we can observe that, whereas MP2 slightly overestimates the binding energy, it is significantly underestimated by DFT, at least when using the B3LYP functional. Nevertheless, the calculated DFT interaction energy is in reasonable agreement with the −5.4 kcal/mol value determined by Cimino et al. at the PNE0/NO6 level for the complex TEMPO···IC_3F_7,[40,41] confirming that changing functional and basis set does not lead to a quantitative agreement with experimental data. Romaniello and Lelj,[36] who studied theoretically the interaction between CF_3I and $(CH_3)_3NO$, attributed the high stability observed for this complex, with respect to corresponding P and S oxides, to electron donation from the O atom to I. The energy they calculated for the $(CH_3)_3NO$··· ICF_3 complex at the scalar relativistic ZORA DFT BP level was 7.81 kcal/mol, which was mainly due to a strong orbital interaction.

Global charge transfers (CT) to ICF_3 determined using Mulliken and NPA, together with those calculated with the molecular electrostatic potential fitted method (Chelpg)[42] are reported in Table 4. In general, CT values determined using

TABLE 4: Binding Energies and Charge Transfers (CT) from TEMPO to ICF_3 Calculated at Different Levels of Theory for the TEMPO···ICF_3 Complex in Vacuum[a]

	TEMPO·ICF_3			
level of theory	ΔE (kcal/mol)	CT [e] Mulliken	CT [e] ChelpG	CT [e] NPA
UB3LYP/SDD[b]	−7.26	0.076	0.163	0.017
UB3LYP/aug-cc-pVDZ[c]//UB3LYP/SDD	−3.83	0.071	0.144	0.010
UB3LYP/aug-cc-pVDZ[b,c]	−4.07	0.026	0.115	0.004
UB3LYP/aug-cc-pVDZ[d]//UB3LYP/SDD	−3.54	−0.028	0.146	0.010
UB3LYP/aug-cc-pVDZ[b,d]	−5.70	−0.032	0.116	0.003
UB3LYP/aug-cc-pVTZ[e]//UB3LYP/SDD	−3.17	0.002	0.148	0.024
UB3LYP/aug-cc-pVTZ[b,e]	−3.37	0.034	0.115	0.011
UMP2/SDD//UB3LYP/SDD	−8.25 (−11.31)	0.035	0.170	0.015
UMP2/aug-cc-pVDZ[c]//UB3LYP/SDD	−6.80 (−11.90)	−0.005	0.148	0.005
UMP2/aug-cc-pVTZ[e]//UB3LYP/SDD	−8.55 (−9.46)	0.019	0.152	0.009

[a] Energies (kcal/mol) not corrected for BSSE for DFT calculations, while BSSE are included in MP2 energies (BSSE uncorrected energies between parentheses). [b] Geometry and energy optimized at the same level of theory. [c] aug-cc-pVDZ on all atoms and I with Stuttgart Dresden ECP. [d] aug-cc-pVDZ on all atoms and I with all electron 6-311G(d) (ref 34). [e] aug-cc-pVTZ on all atoms (refs 30 and 33).

TABLE 5: Binding Energies and Charge Transfers (CT) from TEMPO to ICF_3 Calculated at Different Levels of Theory for the TEMPO·ICF_3 Complex in a $CHCl_3$ Solution Using the IEFPCM Model[a]

	TEMPO·ICF_3			
level of theory	ΔE (kcal/mol)	CT [e] Mulliken	CT [e] ChelpG	CT [e] NPA
UB3LYP/SDD//UB3LYP/SDD^{gas}	−5.46	0.085	0.174	0.019
UB3LYP/SDD[b]	−5.58	0.099	0.181	0.022
UB3LYP/aug-cc-pVDZ[c]//UB3LYP/SDD^{gas}	−3.61	0.081	0.156	0.012
UB3LYP/aug-cc-pVDZ[b,c]	−3.46	0.041	0.128	0.005
UB3LYP/aug-cc-pVTZ[d]//UB3LYP/SDD^{gas}	−1.76	0.008	0.161	0.012

[a] Energies not corrected for BSSE and ZPE and reported in kcal/mol. [b] Geometry and energy optimized at the same level of theory. [c] aug-cc-pVDZ on all atoms and I with Stuttgart Dresden ECP. [d] aug-cc-pVTZ on all atoms (refs 30 and 33).

the Mulliken population analysis are less reliable than those determined with the NPA or the Chelpg method. It can be, in fact, observed that in some cases Mulliken CT predicts that ICF_3 acquires a positive charge, which is contrary to the nature of the binding process for the system under study. Similar inconsistencies were observed previously for NH_3···XR (X = Cl, Br, I) complexes.[43] Chelpg and NPA reproduce more consistently the expected CT trend, giving results in qualitative agreement, though quantitatively different. This difference has already been observed in the literature in the ab initio study of similar complexes, with some authors indicating the Chelpg method as the one that best reproduces experimental data,[44] and others suggesting that it significantly overestimates experimental data and thus preferring to it the NPA.[43] In the present study we will discuss the properties of the TEMPO·ICF_3 bond considering NPA charge transfers. A first observation is that both MP2 and DFT theories predict similar charge transfers when calculations are performed with the same basis set. This suggests that electron densities calculated at the two levels of theory are similar. It is also interesting to observe that reoptimization of the complex structure using a larger basis set leads to a decrease of CT, to which generally corresponds an increase of the NO···I distance. Following Cimino et al.,[41] CT can be interpreted in terms of transfer of charge from the oxygen lone pairs to the C−I orbitals. However, the NPA of the oxygen valence orbitals occupancy shows that the formation of the complex leads to an increase of the O orbital occupation from 6.41 to 6.44 (B3LYP/aug-cc-pVTZ), entirely due to the increase of population of the oxygen 2p orbital, whereas the overall charge transfer is determined by a global decrease of the charge of TEMPO atoms, with N valence population going from 4.96 to 4.94. This can be interpreted observing that the formation of the XB is accompanied by the stabilization of the second resonant structure of TEMPO, followed by CT to the halo-PFC. MP2 calculations with the aug-cc-pVTZ basis set confirm this trend, with predicted O orbital populations of 6.33 and 6.45 in TEMPO and in the complex, respectively. The NPA shows that the observed TEMPO charge polarization is accompanied by a similar, but opposite, polarization of the halo-PFC, as the I charge increases in the complex from 0.1005 to 0.1480, whereas fluorine charges decrease from −0.328 to −0.338.

In order to investigate the influence of the solvent on the occurrence of XB, we determined binding energies for the solvated TEMPO·ICF_3 complex by using the integral equation formalism polarizable continuum model (IEFPCM)[45] and different basis sets. The data are collected in Table 5.

As can be observed from the comparison between the data reported in Tables 4 and 5, solvation in a rather nonpolar solvent such as $CHCl_3$ generally decreases the estimated binding energies, at parities of basis sets. Interestingly, this corresponds to an increase of CT and a decrease of the NO···I distance (from 2.813 to 2.745 Å at the B3LYP/SDD level), which indicates that solvation increases the strength of the NO···I bond, but not as much as it contributes to stabilizing the dissociated molecules. This is reasonable as it is likely that the second resonance structure of TEMPO (Scheme 3), which is more polar than the first, is stabilized by the interaction with the solvent, thus decreasing its tendency to form intermolecular bonds. Finally, it can be observed that if we correct the MP2/aug-cc-pVTZ gas-phase TEMPO···ICF_3 interaction energy with the gas-phase−solution decrease of binding energy computed for DFT, which is about 1.5 kcal/mol, our best prediction of interaction energy in solution becomes about 7.1 kcal/mol, which is similar to the 7 ± 0.4 kcal/mol experimentally measured.[24]

The analysis of the TEMPO·ICF_3 system lead us to conclude that the electronic density distribution, in terms of orbital population and charge transfer, is described similarly both by B3LYP and MP2 theories, though DFT underestimates signifi-

TABLE 6: Isotropic ^{13}C and ^{1}H Chemical Shifts Calculated at the B3LYP Level in Vacuum with Three Basis Sets for the TEMPO Radical[a]

	TEMPO										
	B3LYP IGLO-II			B3LYP IGLO-III			B3LYP aug-cc-pVTZ[b]			exptl[c]	calcd[d]
atom	σ_{iso}^{orb}	σ_{iso}^{con}	δ^{e}	σ_{iso}^{orb}	σ_{iso}^{con}	δ^{e}	σ_{iso}^{orb}	σ_{iso}^{con}	δ^{e}	δ	δ
C1−C2	111.6	864.3	−848.6	107.8	953.9	−937.7	112.4	860.0	−844.7	−1061	−764
C3−C4ax	155.1	−1664.3	1661.2	152.9	−1761.1	1757.9	157.2	−1667.2	1664.3	1462	1361
C3−C4eq	150.7	−764.7	759.2	148.3	−801.3	795.7	152.6	−766.1	760.8		
C6−C7	140.1	−143.2	144.8	137.2	−158.5	160.1	141.7	−149.7	151.5	249	205
C5	162.1	66.8	−68.4	159.6	70.4	−72.1	163.0	67.5	−68.7	−95	−67
Hα	30.9	13.8	−20.0	30.6	13.3	−19.7	30.1	13.3	−19.7	−21	−12.5
$H\alpha^{I}$	30.4	25.8	−31.5	30.1	25.8	−31.7	29.8	25.8	−31.8	−31.8	−25.7
$H\alpha^{II}$	30.4	−10.8	5.0	30.1	−11.1	5.2	29.8	−10.0	4.7	6.7	2.7

[a] Data expressed in ppm and compared with experimental measurements and previous theoretical data. Numbering of atoms with reference to Figure 1. [b] aug-cc-pVTZ on all atoms (refs 30 and 33). [c] Hatch and Kreilick (ref 49) for ^{13}C and Kreilick (ref 50) for ^{1}H. [d] Calculated with density functional theory using the BP86 functional (ref 47). [e] Chemical shift calculated with reference to the ^{13}C chemical shift of 2,2,6,6-tetramethylpiperidine, in order to be consistent with experimental data; ^{1}H chemical shift referred to benzene. σ_{iso}^{ref} for ^{13}C was the following (ppm): C1−C2 127.3 (IGLO-II), 124.0 (IGLO-III), 127.7 (aug); C3−C4ax 152.1 (IGLO-II), 149.7 (IGLO-III), 154.4 (aug); C3−C4eq 145.3 (IGLO-II), 142.7 (IGLO-III), 147.4 (aug); C4−C6 141.7 (IGLO-II), 138.8 (IGLO-III), 143.5 (aug); C5 160.6 (IGLO-II), 157.9 (IGLO-III), 161.8 (aug); H 24.9 (IGLO-II), 25.3 (IGLO-III), 24.1 (aug).

cantly experimental binding energies. However, it is known that NMR properties calculated with DFT are usually in good agreement with experimental data.[46] Considering the more favorable scaling of DFT computational requirements with basis set size with respect to MP2, we decided to determine paramagnetic nuclear magnetic properties of TEMPO and of the TEMPO·ICF_3 complex in vacuum using DFT, and in particular the B3LYP functional, with three basis sets, the IGLO-II, and IGLO-III basis sets incremented with sp diffuse functions[51] and the aug-cc-pVTZ basis set, on structures optimized at the B3LYP/aug-cc-pVTZ level of theory.

The nuclear magnetic shielding tensor was calculated as suggested by Pennanen and Vaara[46] as

$$\sigma_K = \sigma_K^{orb} - \frac{1}{\gamma_K}\frac{\mu_B}{3kT}S(S+1)\mathbf{g}\cdot\mathbf{A_K} \quad (1)$$

where μ_B is the Bohr magneton, S is the electronic spin, σ_K^{orb} is the orbital shielding tensor, and $\mathbf{g}$ and $\mathbf{A_K}$ are the g and hyperfine coupling tensors, respectively. The temperature-dependent term derives from the degeneracy of the electronic spin S, which leads to the presence of multiple states, the occupation of which can be determined assuming a Boltzmann distribution. The paramagnetic contribution to the shielding constant derives therefore by the interaction of electronic and nuclear spins with the magnetic field. The $\mathbf{g}\cdot\mathbf{A_K}$ product can be expanded in the sum of several terms, which go from the Fermi contact interaction to the dipolar interaction, to other terms deriving from relativistic spin orbit contributions. Since, as shown recently,[47] the leading term is the isotropic Fermi contact interaction, we limited our computational study to the evaluation of the σ_K^{orb} orbital shift with the gauge-independent atomic orbital method (GIAO)[48] and correct it for the paramagnetic interaction by adding the contact term calculated using the nonrelativistic hyperfine coupling tensor σ_{iso}^{con}. Summarizing, we computed the chemical shift as

$$\delta = \sigma_{iso}^{ref} - \sigma_{iso}^{orb} - \sigma_{iso}^{con} \quad (2)$$

where σ_{iso}^{orb} is the shielding constant of the reference diamagnetic compound, which, for the fluorine atom, was $CFCl_3$, tetramethylpiperidine for carbon, and benzene for hydrogen. GIAO shielding tensors and hyperfine coupling tensors were calculated in vacuum both at the B3LYP/IGLO-II, B3LYP/IGLO-III, and at the B3LYP/aug-cc-pVTZ levels on geometries optimized at the B3LYP/aug-cc-pVTZ level. The IGLO basis set family was preferred to the SDD basis set as it is more apt to calculate NMR properties. The isotropic components of the magnetic shielding tensor for key atoms and chemical shifts calculated at two levels of theory are reported in Table 6 for the TEMPO radical.

Computed and experimental ^{13}C chemical shifts are in a good qualitative agreement, which becomes quantitative for H chemical shifts. The shift determined by Fermi contact interactions affects considerably both the C and H chemical shifts, in particular for what concerns axial carbon atoms. The chemical shift of methyl hydrogens was averaged between axial and equatorial positions, since, as reported by Hatch and Kreilick,[49] the TEMPO radical interconverts rapidly on the proton NMR time scale, while the same interconversion is much slower on the carbon NMR time scale so that equatorial and axial carbon atoms are not equivalent. It is also worth observing that the measured C shift is significantly influenced by the solvent nature and the solute concentrations so that the significant quantitative disagreement between experimental and calculated carbon shift might in part be because our simulations were performed in vacuum.

Chemical shifts calculated for the TEMPO·ICF_3 complex are reported in Table 7. The addition of ICF_3 modifies significantly the ^{13}C shifts with respect to those of the TEMPO radical. The NPA of the fluorine atoms evidence that the isotropic contribution is proportional to the difference between the population of their α and β valence orbitals and, thus, to spin transfer from TEMPO. Comparing the ^{19}F chemical shifts of Table 7 with those of pure ICF_3, which are −3.5 ppm, −9.3 ppm, and −13.0 ppm at the B3LYP/IGLO-II, B3LYP/IGLO-III, and B3LYP/aug-cc-pVTZ levels, respectively, we can conclude that the formation of the TEMPO·ICF_3 halogen-bonded complex leads to a relative change of the F chemical shifts by −6.5, −10.9, and −7.8 ppm at the three levels of theory. The calculated values are in good agreement with experimental data (−7.22 ppm, see Table 2). Also, as DFT calculations in implicit solvent have shown that CT increases in solution, it is likely that the calculated shift is underestimated. This negative shift, which is a peculiar characteristic of complexes formed by iodo-PFCs with the TEMPO radical and is not observed in complexes with

TABLE 7: Isotropic ^{13}C, ^{1}H, and ^{19}F Chemical Shifts Calculated with Density Functional Theory at the B3LYP Level with Three Basis Sets for the TEMPO·ICF_3 Complex and Spin Densities Calculated at the B3LYP/aug-cc-pVTZ Level[a]

	TEMPO·ICF_3 Complex									
	B3LYP/IGLO-II			B3LYP/IGLO-III			B3LYP/aug-cc-pVTZ[b]			
atom	σ_{iso}^{orb}	σ_{iso}^{con}	δ^c	σ_{iso}^{orb}	σ_{iso}^{con}	δ^c	σ_{iso}^{orb}	σ_{iso}^{con}	δ^c	spin density
C1−C2	110.5	995.6	−978.8	106.7	1086.0	−1068.7	111.1	975.9	−959.3	−0.021
C3−C4ax	155.2	−1836.2	1833.1	152.9	−1849.1	1845.9	157.0	−1837.4	1834.8	0.029
C3−C4eq	151.1	−798.3	792.6	148.5	−2348.1	2342.3	152.3	−796.9	792.0	0.009
C4−C6	140.2	−160.8	162.3	137.1	−499.0	500.7	142.0	−168.8	170.3	0.002
C5	162.5	67.8	−69.7	159.9	205.5	−207.5	163.2	67.5	−68.9	-4.7×10^{-3}
F1−F3	180.2	5.2	3.0	175.9	−19.3	1.55	185.3	−16.8	−5.2	1.3×10^{-4}

[a] NMR shifts are expressed in ppm. Numbering of atoms with reference to Figures 1 and 2. [b] aug-cc-pVTZ on all atoms (refs 30 and 33). [c] Chemical shift calculated with reference to the ^{13}C chemical shift of 2,2,6,6-tetramethylpiperidine are the same as reported in Table 3; ^{19}F chemical shift with reference to $CFCl_3$: 168.0 (B3LYP/IGLO-II), 158.2 (B3LYP/IGLO-III), 163.3 (B3LYP/aug-ccpVTZ).

closed shell N and O containing molecules, is determined by the paramagnetic contribution to the shielding tensor. Since the paramagnetic leading term is the Fermi contact isotropic interaction, which is proportional to the atomic spin density, we can conclude that the origin of the downshift of the ^{19}F NMR signal is the spin transfer from TEMPO to ICF_3. This spin transfer has been unequivocally demonstrated at the experimental level by our previous EPR studies on complexes of TEMPO with iodo-PFCs.[24] The conclusion mentioned above is supported by the spin density calculated as difference between the natural population of α and β orbitals of the TEMPO·ICF_3 complex with the aug-cc-pVTZ basis set and shown in the last column of Table 7.

3. Summary and Conclusions

The influence of the formation of halogen-bonded adducts with a prototype nitroxide radical, TEMPO, on the ^{19}F NMR spectra of the haloperflurocarbons involved has been experimentally and computationally investigated.

Experimentally, it was found that the addition of the paramagnetic molecule to solutions containing 1-haloperfluoroalkanes influences significantly the resonances of the signals of the $-CF_2-X$ groups, which are substantially downfield shifted. This clearly contrasts with what is usually observed for the ^{19}F NMR spectra of haloperfluorocarbons halogen bonded to diamagnetic molecules, where marked upfield shifts are generally measured. The key role of the halogen bonding with TEMPO in the induction of such a specific paramagnetic shift is demonstrated by the systematic decrease of the intensity of the downfield shift with the polarizability of the halogen, according to the decrease of the halogen bonding strength. As a further confirmation of this, the shifts of the signals of the $-CF_2-$ group geminal to the halogen atoms involved in the specific interactions are invariably larger than the shifts of the other $-CF_2-$ groups, these shifts decreasing with increasing distance from the electron acceptor halogen atoms. To the best of our knowledge, this is the first report on the use of stable free radicals as ^{19}F NMR spin probes for studying intermolecular interactions involving halo-PFCs, and it could be envisaged that this method will help in the characterization of halogen bonding interactions, which are a relatively new tool for assembling molecular materials.

The physicochemical origin of the downfield shift was, then, theoretically investigated performing ab initio and density functional theory simulations of the TEMPO·ICF_3 complex. It was found that the formation of the halogen bond is accompanied by a significant charge polarization of both molecules, and in particular, of the most polar resonance structure of TEMPO. The best estimation of the gas-phase binding energy of the complex, obtained at the MP2/aug-cc-pVTZ level, is about −8.55 kcal/mol, which is expected to decrease to about −7 kcal/mol in a $CHCl_3$ solution, which is in good agreement with experimental data. DFT calculations significantly underestimate the binding energy, though charge transfer is predicted similarly by both DFT and MP2 calculations when large basis sets are adopted. ^{19}F NMR chemical shifts were determined correcting the isotropic diamagnetic shift for contact interactions determined from the hyperfine coupling tensor. A good agreement with the experimental data was found using structures optimized at a high level of theory and different basis sets. The origin of the downfield shift could thus clearly be ascribed to paramagnetic contributions determined by Fermi contact interactions and, thus, to spin transfer from TEMPO to the ICF_3 fluorine atoms.

Acknowledgment. This work is partially supported by Fondazione Cariplo (Project "Self-Assembled Nanostructured Materials: A Strategy for the Control of Electrooptic Properties"). The COST D31/0017/05 project is also gratefully acknowledged. The authors thank one of the referees for the useful advice, which helped to improve the quality of this paper.

Supporting Information Available: Experimental NMR procedures and graphs, atomic coordinates of TEMPO and of the TEMPO·ICF_3 complex. This material is available free of charge via the Internet at http://pubs.acs.org.

References and Notes

(1) Lu, Y. X.; Zou, J. W.; Wang, Y. H.; Zhang, H. X.; Yu, Q. S.; Jiang, Y. J. *J. Mol. Struct. (THEOCHEM)* **2006**, *766*, 119.

(2) Lohr, H.-G.; Engel, A.; Josel, H.-P.; Vogale, F.; Schuh, W.; Puff, H. *J. Org. Chem.* **1984**, *49*, 1621.

(3) Awwadi, F. F.; Willett, R. D.; Peterson, K. A.; Twamley, B. *Chem. Eur. J.* **2006**, *12*, 8952.

(4) Karpfen, A. In *Halogen Bonding Fundamentals and Applications*; Metrangolo, P., Resnati, G., Eds.; Spinger: Berlin and Heidelberg, 2008; p 1.

(5) Clark, T.; Hennemann, M.; Murray, J. S.; Politzer, P. *J. Mol. Model.* **2007**, *13*, 291.

(6) Landrum, G. A.; Goldberg, N.; Hoffmann, R. *J. Chem. Soc., Dalton Trans.* **1997**, 3605.

(7) Lommerse, J. P. M.; Stone, A. J.; Taylor, R.; Allen, F. H. *J. Am. Chem. Soc.* **1996**, *118*, 3108.

(8) Metrangolo, P.; Neukirch, H.; Pilati, T.; Resnati, G. *Acc. Chem. Res.* **2005**, *38*, 386.

(9) Metrangolo, P.; Resnati, G.; Pilati, T.; Biella, S. In *Halogen Bonding Fundamentals and Applications*; Metrangolo, P., Resnati, G., Eds.; Springer: Berlin and Heidelberg, 2008; p 105.

(10) Metrangolo, P.; Resnati, G. *Chem. Eur. J.* **2001**, *7*, 2511.

(11) Gonnade, R. G.; Shashidhar, M. S.; Bhadbhade, M. M. *Indian Inst. Sci.* **2007**, *87*, 149.

(12) Metrangolo, P.; Meyer, F.; Pilati, T.; Resnati, G.; Terraneo, G. *Angew. Chem., Int. Ed.* **2008**, *47*, 6114.
(13) Messina, M. T.; Metrangolo, P.; Panzeri, W.; Ragg, E.; Resnati, G. *Tetrahedron Lett.* **1998**, *39*, 9069.
(14) Metrangolo, P.; Panzeri, W.; Recupero, F.; Resnati, G. *J. Fluorine Chem.* **2002**, *114*, 27.
(15) Morishima, I.; Inubushi, T.; Endo, K.; Yonezawa, T. *Chem. Phys. Lett.* **1972**, *14*, 372.
(16) Morishima, I.; Inubushi, T.; Endo, K.; Yonezawa, T.; Goto, G. *J. Am. Chem. Soc.* **1972**, *94*, 4812.
(17) Morishima, I.; Inubushi, T.; Yonezawa, T. *J. Am. Chem. Soc.* **1976**, *98*, 3808.
(18) Iwasaki, F.; Yoshikawa, J. H.; Yamamoto, H.; Kan-Nari, E.; Takada, K.; Yasui, M.; Ishida, T.; Nogami, T. *Acta Crystallogr., Sect. B* **1999**, *55*, 231.
(19) Boubekeur, K.; Syssa-Magale, J. L.; Palvadeau, P.; Schollhorn, B. *Tetrahedron Lett.* **2006**, *47*, 1249.
(20) Wagner, B.; Gommper, R.; Polborn, K. Personnal communication, 2002, CCDC 198532 (CSD VADFOW).
(21) Hosokoshi, Y.; Tamura, M.; Nozawa, K.; Suzuki, S.; Kinoshita, M.; Sawa, H.; Kato, R. *Synth. Met.* **1995**, *71*, 1795.
(22) Zakrassov, A.; Shteiman, V.; Sheynin, Y.; Botoshansky, M.; Kapon, M.; Kaftory, M.; Del Sesto, R. E.; Miller, J. S. *Helv. Chim. Acta* **2003**, *86*, 1234.
(23) Tamura, M.; Shiomi, D.; Hosokoshi, Y.; Iwasawa, N.; Nozawa, K.; Kinoshita, M.; Sawa, H.; Kato, R. *Mol. Cryst. Liq. Cryst.* **1993**, *232*, 45.
(24) Mugnaini, V.; Punta, C.; Liantonio, R.; Metrangolo, P.; Recupero, F.; Resnati, G.; Pedulli, G. F.; Lucarini, M. *Tetrahedron Lett.* **2006**, *47*, 3265.
(25) Qui, Z. W.; Grant, D. M.; Pugmire, R. J. *J. Am. Chem. Soc.* **1982**, *104*, 2747.
(26) Qui, Z. W.; Grant, D. M.; Pugmire, R. J. *J. Am. Chem. Soc.* **1984**, *106*, 557.
(27) Bonesteel, J. K.; Al-Bala'a, I., Jr *Bull. Magn. Res.* **1993**, *15*, 18.
(28) Sysoeva, N. A.; Karmilov, A. Y.; Buchachenko, A. L. *Chem. Phys.* **1976**, *15*, 321.
(29) Dunning, T. H.; Hay, P. J. In *Modern Theoretical Chemistry*; Schaefer, H. F., Ed.; Plenum: New York, 1976; p 1.
(30) Woon, D. E.; Dunning, T. H. *J. Chem. Phys.* **1993**, *98*, 1358.
(31) Foster, J. P.; Weinhold, J. *J. Am. Chem. Soc.* **1980**, *102*, 7211.
(32) Fuentealba, P.; Preuss, H.; Stoll, H.; Szentpaly, L. V. *Chem. Phys. Lett.* **1989**, *89*, 418.
(33) Martin, J. M. L.; Sundermann, A. *J. Chem. Phys.* **2001**, *114*, 3408.
(34) Glukhovtsev, M. N.; Pross, A.; McGrath, M. P.; Radom, L. *J. Chem. Phys.* **1995**, *103*, 1878.
(35) Valerio, G.; Raos, G.; Meille, S. V.; Metrangolo, P.; Resnati, G. *J. Phys. Chem. A* **2000**, *104*, 1617.
(36) Romaniello, P.; Lelj, F. *J. Phys. Chem. A* **2002**, *106*, 9114.
(37) Boys, S. *Mol. Phys.* **1970**, *19*, 553.
(38) Xantheas, S. S. *J. Chem. Phys.* **1996**, *104*, 8821.
(39) Frisch, M. J.; Trucks, G. W.; Schlegel, H. B.; Scuseria, G. E.; Robb, M. A.; Cheeseman, J. R.; Montgomery, J. A., Jr.; Vreven, T.; Kudin, K. N.; Burant, J. C.; Millam, J. M.; Iyengar, S. S.; Tomasi, J. J.; Barone, V.; Mennucci, B.; Cossi, M.; Scalmani, G.; Rega, N.; Petersson, G. A.; Nakatsuji, H.; Hada, M.; Ehara, M.; Toyota, K.; Fukuda, R.; Hasegawa, J.; Ishida, M.; Nakajima, T.; Honda, Y.; Kitao, O.; Nakai, H.; Klene, M.; Li, X.; Knox, J. E.; Hratchian, H. P.; Cross, J. B.; Adamo, C.; Jaramillo, J.; Gomperts, R.; Stratmann, R. E.; Yazyev, O.; Austin, A. J.; Cammi, R.; Pomelli, C.; Ochterski, J. W.; Ayala, P. Y.; Morokuma, K.; Voth, A.; Salvador, P.; Dannenberg, J. J.; Zakrzewski, V. G.; Dapprich, S.; Daniels, A. D.; Strain, M. C.; Farkas, O.; Malick, D. K.; Rabuck, A. D.; Raghavachari, K.; Foresman, J. B.; Ortiz, J. V.; Cui, Q.; Baboul, A. G.; Clifford, S.; Cioslowski, J.; Stefanov, B. B.; Liu, G.; Liashenko, A.; Piskorz, P.; Komaromi, I.; Martin, R. L.; Fox, D. J.; Keith, T.; Al-Laham, M. A.; Peng, C. Y.; Nanayakkara, A.; Challacombe, M.; Gill, P. M. W.; Johnson, B.; Chen, W.; Wong, M. W.; Gonzalez, C.; Pople, J. A. *Gaussian 03*, revision C.01; Gaussian, Inc.: Pittsburgh, PA, 2003.
(40) Cimino, P.; Pavone, M.; Barone, V. *Chem. Phys. Lett.* **2006**, *419*, 106.
(41) Cimino, P.; Pavone, M.; Barone, V. *J. Phys. Chem. A* **2007**, *111*, 8482.
(42) Breneman, C. M.; Wiberg, K. B. *J. Comput. Chem.* **1990**, *11*, 361.
(43) Zou, J. W.; Jiang, Y. J.; Guo, M.; Hu, G. X.; Zhang, B.; Liu, H. C.; Yu, Q. S. *Chem. Eur. J.* **2005**, *11*, 740.
(44) Szefczyk, B.; Sokalski, W. A.; Leszczynski, J. *J. Chem. Phys.* **2002**, *117*, 6952.
(45) Cances, E.; Mennucci, B.; Tomasi, J. *J. Chem. Phys.* **1997**, *107*, 3032.
(46) Pennanen, T. O.; Vaara, J. *J. Chem. Phys.* **2005**, *123*, 174102.
(47) Rinkevicius, Z.; Vaara, J.; Telyatnyk, L.; Vahtras, O. *J. Chem. Phys.* **2003**, *118*, 2550.
(48) Wolinski, K.; Hinton, J. F.; Pulay, P. *J. Am. Chem. Soc.* **1990**, *112*, 8251.
(49) Hatch, G. F.; Kreilick, R. W. *J. Chem. Phys.* **1972**, *57*, 3696.
(50) Kreilick, R. W. *J. Chem. Phys.* **1966**, *46*, 4260.
(51) Kutzelnigg, W.; Fleischer, U.; Schindler, M. In *NMR Basic Principles and Progress*; Diehl, P., Fluck, E., Gunther, H., Kosfeld, R., Eds.; Springer-Verlag: Heidelberg, 1990; Vol. 23.

JP803685R